WILEY-VCH

SUPPORTING INFORMATION

Supporting Information

69451 Weinheim, Germany

Kinetic Microscale Thermophoresis

Julian A. C. Stein, Alan Ianeselli, Dieter Braun*

Abstract: We established an extension of Microscale Thermophoresis (MST) to measure binding kinetics together with binding affinity in a single experimental run, by increasing the thermal dissipation of the sample. After the switch-off of an IR laser, that locally heated the sample, the temperature re-equilibrated within 250 ms. The kinetic relaxation fingerprints were extracted from the fluorescence changes back to thermodynamic equilibrium. We measured DNA hybridization on-rates and off-rates in the range between 10^{4}-10^{6} $M^{-1}s^{-1}$ and 10^{-4}-10^{-1} s^{-1}, respectively. We observed the expected exponential dependence of the DNA hybridization off-rates on salt concentration, strand length and inverse temperature. The measured on-rates showed a linear dependence on salt and weak if no dependence at all on length and temperature. For biological binding reactions with sufficient enthalpic contributions, Kinetic MST offers a robust and immobilization-free determination of kinetic rates and binding affinity and also in crowded solutions.

DOI: 10.1002/anie.2016XXXXX

Table of Contents

Experimental Procedures

1 Experimental setup

All KMST measurements were carried out with a Nanotemper Monolith(R) NT.115 Pico. Each sample of the dilution series was filled in a high precision round borosilicate glass capillary ID300µm, OD400µm, (Hollow Round Glass Capillaries, CM Scientific). The fluorescence excitation/detection unit of the NT.115 Pico measured the fluorescence intensity change with the RED filter set (excitation 605-645 nm, emission 660-710 nm) over the whole experiment time in a localized spot with a spatial range of about 20 µm.

The heating of the sample to the final temperature showed an exponential time-characteristic, with the inverse heating time constant τ_{heat}^{-1}, see SI-Fig.1 a & b. For MST measurements with conventional sample holder the capillary was freely-lying in air. The inverse heating time was $\tau_{heat}^{-1} = 0.38\, s^{-1}$, which corresponds to at heating time of 2.6 seconds. This results from the rather weak thermal coupling of the capillaries with the surrounding air and turned out to be is too slow for KMST detection.

To enable the detection of kinetic fingerprints, the thermal coupling of a KMST setup was strongly increased in comparison to an MST setup: first, the samples were loaded into smaller round glass capillaries with an inner diameter of 300µm OD 400µm, instead of conventionally used 500µm ID, 1000µm OD. Second, the commercially available sample holder for the NT.115 Pico was slightly modified: Instead of being surrounded by air, the capillaries containing the sample solutions were placed on a thin silicon wafer. Third, the capillaries on the silicon wafer were immersed with oil (Zeiss Immersion Oil 518 F). Fourth, a thin glass cover slip (Carl Roth) is placed on top of all capillaries, see Fig.1 a & b and SI-Fig.1 d. The covering of the capillaries by immersion oil and the glass cover slip yielded for an equal heat transfer and for a homogeneous fluorescence detection for of the 16 capillaries within the assay, respectively (not shown). For this, a thin section had to be milled out from top of the aluminum sample holder. The high thermal conductivity of the modified KMST setup provided much faster heat transfer from the heated sample to the environment and the inverse heating time increases to about $\tau_{heat}^{-1} > 4\, s^{-1}$, corresponding to <250 ms heating time. It is an order of magnitude faster in comparison to a standard sample holder, see SI-Fig.1 b. It is also an order of magnitude faster than the fastest kinetic relaxation time.

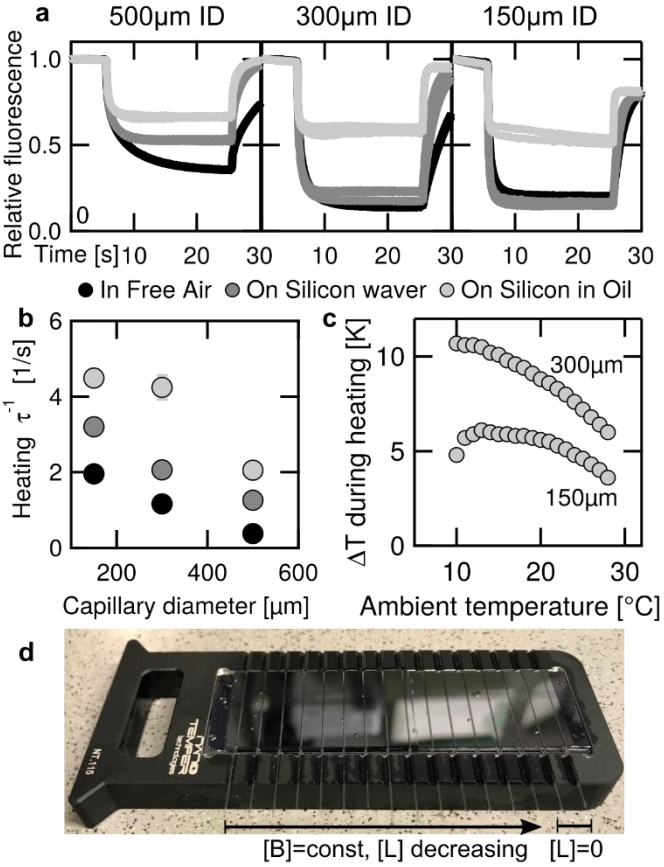

SI-Figure 1: Sample heating characteristics a *Relative fluorescence over time of Cy-5 in 1xPBS solution during heating for various capillary sizes (500µm, 300µm and 150µm inner diameter) and sample holder specifications.* ***b*** *The strong heat-coupling of the sample to the Silicon-Oil-Coverslip holder (SOC) enables for short high inverse heating times.* ***c*** *the temperature jump during the hot time is about 10K for capillaries with inner diameter 300µm.* ***d*** *The SOC sample holder with capillaries filled with constant binder and decreasing ligand concentrations - from left to right*

To determine the amplitude of the temperature jump during the heating, the fluorescence dependence of the dye was measured for temperatures between 10°C and 28°C. The absolute fluorescence of Cy5-only samples (biomers GmbH, Ulm, Germany, 10 nM in 0.1xPBS buffer, Ambion) during the hot time are related to the initial fluorescence at the measured ambient temperatures. The absolute

fluorescence for the hot time depended linearly on the ambient temperature for labeled DNA and Cy5 only in the measured range 10°C to 28°C (not shown). The amplitude of the temperature jump is shown in SI.Fig.1 c for various ambient temperatures. We found a temperature jump of about $\Delta T = 10\ K$ for 300µm ID round capillaries and $\Delta T = 6\ K$ for 150 µm capillaries for Cy5-only measurements. These temperature jumps were the average over the detection volume. Measurements of samples with the Cy5-labeled 12mer DNA strand showed a highly similar behavior (not shown). Due to restrictions of the adjustment of the ambient temperature, all obtained hot time values above 20°C were made on the assumption that the fluorescence changes from cold to hot decreased linearly with temperature.

The use of smaller capillaries led to less pronounced convection effects, which interfere with the measurement of kinetics in the following way: During heating, the movement of (bleached) fluorescent molecules out of the (warmer) illuminated region towards the (colder) non-illuminated region and the influx of non-bleached fluorescent molecules into the heated region change the fluorescence independently from kinetic processes. When the laser was switched off, fluorescent molecules from formerly not heated regions could diffuse back into the illuminated region and change the detected fluorescence. Small capillaries reduced these effects. The small capillary size also decreased the thermophoretic effect due to more shallow temperature gradients.

2 Binding curve from bleaching rates

The in equilibrium, the reaction of a labeled binder B* and ligand L$L + B^* \Leftrightarrow LB^*$can be characterized by $K_d = \frac{L \cdot B^*}{LB^*} = \frac{k_{off}}{k_{on}}$ with L the free ligand and B* the free binder concentrations and LB* the bound complex concentration. Note that the concentrations of free L and free B* are in general not experimentally accessible, but only the total ligand concentration L_{tot} and total binder concentration B^*_{tot}. The on-rate k_{on} and off-rate k_{off} correspond to the respective equilibrium conditions. The fraction of bound complex P_{bound}=LB*/B^*_{tot} can be expressed by[1]

$$P_{bound} = \frac{LB^*}{B^*_{tot}} = \frac{L_{tot} + B^*_{tot} + K_d - \sqrt{\left(L_{tot} + B^*_{tot} + K_d\right)^2 - 4L_{tot} \cdot B^*_{tot}}}{2B^*_{tot}} \qquad (1)$$

The measured bleaching rates k_{bleach} are related to the fraction bound by

$$P_{bound} = \frac{k_{bleach} - k_{bleach,bound}}{k_{bleach,free} - k_{bleach,bound}}$$

Thus, the fitting the measured bleaching rates to the total ligand concentrations yields for the fraction bound, K_d, $k_{bleach,\ free}$ and $k_{bleach,\ bound}$. [2] As documented in the works of Schoen[3] a square root-dependence of $\tau^{-1}_{kinetic} = \sqrt{\left(k_{off}\left(k_{off} + 4k_{on}B_{tot}\right)\right)}$ is found for a 1:1 mixture of B_{tot}=L_{tot}. In our case, the mixture ratio deviated from the 1:1 ratio, therefore the relationship had to be adjusted as shown in Eq. 2, pointing to a linear dependence of $\tau^{-1}_{kinetic}$on the ligand concentration L_{tot} with constant binder B_{tot}.

3 Choice of post heat phase for kinetic analysis

In principle, the kinetic rates could be determined by the analysis of the fluorescent traces after both temperature jumps. However, the only analysis of the fluorescence traces during the post heat phase of the second temperature jump was well suitable for two reasons. First, the determination of the kinetic rates with Eq. 2 required the concentrations of the reactants to come back to equilibrium, that is at constant temperature of the sample in the post heat phase. The determination of K_d and the respective binding curve in the pre heat phase only allowed for determination in equilibrium state, which are pre heat and post heat phases (after kinetic equilibration). Second, the fluorescence change during the hot phase due to strong convection and thermophoretic effects superimposed with the fluorescence change due to the kinetic effects and bleaching. The disentanglement of the effects in this phase was difficult. As seen in Fig.2, our numerical model can handle all these effects in a reasonable manner, however these results are not sufficient to perform a full kinetic analysis.

4 Reaction kinetics from fluorescence traces

The on-rate and off-rate of a ligand-binder reaction $L + B \Leftrightarrow LB$ was fitted to the experimentally-accessible kinetic time constant

$$\tau^{-1}_{kinetic} = k_{on}\sqrt{(L_{tot} + B^*_{tot} + K_d)^2 - 4L_{tot} \cdot B^*_{tot}} \quad (2)$$

with the equilibrium constant K_d and the known total binder B^*_{tot} and total ligand L_{tot} concentrations for a second-order reaction process. K_d and the fraction bound in equilibrium $P_{bound,eq}$, were determined by the binding-dependent fluorescence bleaching in the pre heat phase[4] see SI-2. We fitted the on-rate to a dilution series with increasing L_{tot}, constant label concentration B^*_{tot}<K_d and the exponentially fitted $\tau^{-1}_{kinetic}$from the cooling phase. The usage of multiple L_{tot} increased the robustness of the fit due to more measurement points within one single concentration k_{on}-fit.

To access the kinetic relaxation constant $\tau^{-1}_{kinetic}$in the post heat phase, we dissected the kinetic contribution from bleaching and convection terms within the fluorescence signal. We treated the fluorescence signal$F(t)[\#emitted\ photons/second]$per time interval Δt as the integral over the illuminated detection volume dV of the time and space-dependent free $B^*(t,\vec{x})[mol/m^3]$and bound $LB^*(t,\vec{x})[mol/m^3]$ fluorescent molecules – B and LB denote the bleached species which do not contribute to the fluorescence signal:

$$F(t) = \int dV \left(B^*(t,\vec{x}) \cdot \left(F_{Free} + \frac{\partial F_{Free}}{\partial T} \cdot \Delta T\right) + LB^*(t,\vec{x}) \cdot \left(F_{Bound} + \frac{\partial F_{Bound}}{\partial T} \cdot \Delta T\right)\right) \qquad (3)$$

With $F_i\left[\frac{\#\text{emitted photons}}{second \cdot mol}\right]$ the fluorescence quantum efficiencies of bound and free binder states, $\frac{\partial F_i}{\partial T}$ the respective temperature dependence, $\Delta T = T - T_0$ the temperature change compared to the equilibrium temperature T_0. The concentrations of ligand, free and bound (bleached) binder depend on kinetics, diffusive/convective movement and bleaching, see Fig.1 a. For any point $\vec{x}$, the following rate equations apply

$$\begin{aligned}
\dot{L}(t) &= +k_{off} \cdot LB^*(t) - k_{on} \cdot B^*(t) \cdot L(t) + D\Delta L(t) - \nabla\left(L(t) \cdot \left(\vec{u} - D_{T,L} \cdot \nabla T\right)\right) \\
\dot{B^*}(t) &= +k_{off} \cdot LB^*(t) - k_{on} \cdot B^*(t) \cdot L(t) + D\Delta B^*(t) - \nabla\left(B^*(t) \cdot \left(\vec{u} - D_{T,B} \cdot \nabla T\right)\right) - k_{bleach,free} \cdot B^*(t) \\
\dot{LB^*}(t) &= -k_{off} \cdot LB^*(t) + k_{on} \cdot B^*(t) \cdot L(t) + D\Delta LB^*(t) - \nabla\left(LB^*(t) \cdot \left(\vec{u} - D_{T,LB} \cdot \nabla T\right)\right) - k_{bleach,bound} \cdot LB^*(t) \\
\dot{B}(t) &= +k_{off} \cdot LB(t) - k_{on} \cdot B(t) \cdot L(t) + D\Delta B(t) - \nabla\left(B(t) \cdot \left(\vec{u} - D_{T,B} \cdot \nabla T\right)\right) + k_{bleach,free} \cdot B^*(t) \\
\dot{LB}(t) &= -k_{off} \cdot LB(t) + k_{on} \cdot B(t) \cdot L(t) + D\Delta LB(t) - \nabla\left(LB(t) \cdot \left(\vec{u} - D_{T,LB} \cdot \nabla T\right)\right) + k_{bleach,bound} \cdot LB^*(t)
\end{aligned} \quad (4)$$

With $k_{bleach,i}$ the bleaching rates of free and bound state, $D\Delta c - \nabla\left(c(t) \cdot \left(\vec{u} - D_T \cdot \nabla T\right)\right)$ the diffusive, advective and thermophoretic contributions with the diffusion constant D, the thermal diffusion constant D_T and u the velocity field for the respective concentration c. In the following, we rewrite the motion term as $D(t)$, which we approximate to be the same for B^* and LB^*.

To extract the kinetic relaxation constant from the fluorescent traces in the post heating phase, we write the solution B^* and LB^* of the rate equation system (Eq. 4) as a product of the kinetic, bleaching and convective solutions $B^*(t) = B^*_{tot} \cdot B_{kinetic}(t) \cdot B_{bleach}(t) \cdot B_{diffusion}(t)$ and analogously for LB^*. B^* and LB^* are expressed by the total concentration of labeled binder B^*_{tot} with $B^* = B^*_{tot} - LB^*$ and the fraction bound $LB^* = P_{bound}(t) \cdot B^*_{tot}$. The kinetic solution after a quick temperature jump is a second order exponential relaxation

$$B_{kinetic}(t) = 1 - P_{bound}(t) = 1 - \left(P_{bound,eq} - \left(P_{bound,eq} - P_{bound,hot}\right) \cdot exp(-t/\tau_{kinetic})\right) \quad (5)$$

with the fraction bound in equilibrium $P_{bound,eq}$, the fraction bound in the hot phase $P_{bound,hot}$ and the kinetic relaxation constant from Eq. 2. The bleaching term is extracted from the pre heating phase and read $B_{bleach}(t) = exp\left(-t \cdot k_{Bleach,free}\right)$ and $LB_{bleach}(t) = exp\left(-t \cdot k_{Bleach,bound}\right)$. The diffusion term $B_{diffusion}(t)$ is obtained by the zero ligand trace, see below. With $\hat{F}_i = \left(F_i + \frac{\partial F_i}{\partial T} \cdot \Delta T\right) \cdot B^*_{tot}$ the fluorescence in the post heat phase reads:

$$\begin{aligned}
F(t) &= \int dV\, D(t) \cdot (\hat{F}_{Bound}\left(P_{bound,eq} - \left(P_{bound,eq} - P_{bound,hot}\right) \cdot exp(-t/\tau_{kinetic})\right) \cdot exp\left(-t \cdot k_{Bleach,bound}\right) \\
&+ \hat{F}_{Free}\left(1 - \left(P_{bound,eq} - \left(P_{bound,eq} - P_{bound,hot}\right) \cdot exp(-t/\tau_{kinetic})\right)\right) \cdot exp\left(-t \cdot k_{Bleach,free}\right))
\end{aligned} \quad (6)$$

To access the time-dependent kinetic relaxation, the bleaching and diffusion contributions need to be eliminated. The measured data normalized to its initial value, and then Eq. 6 is divided by the exponential bleaching and diffusion contributions to obtain the kinetic term (Eq. 7) to which the exponential relaxation is fitted. Therefore, the effective bleaching rate k_{bleach} as an approximate for the underlying free and bound bleaching rates is obtained from equilibrium by fitting $F_{eq} \approx F_0 exp(-t \cdot k_{bleach})$ to the pre heat phase, see SI-2. Note that the fit for this exponential bleaching does not have an offset, as bleaching converges to 0 for $t \to \infty$.
To eliminate artifacts from the temperature jump, the first 2.1 seconds after the detection of the second temperature jump are cut out. The diffusion term D(t) can be obtained from the zero-ligand fluorescence trace in the post heat phase $F_{Ligand=0}(t) = \int dV \cdot D(t) \cdot \hat{F}_{Free} \cdot exp\left(-t k_{Bleach,free}\right)$. Yet, we only can determine $D(t) \cdot \hat{F}_{Free} \approx F_{ligand=0}/exp\left(-t \cdot k_{Bleach,free}\right)$ which is sufficient for further analysis. Dividing F(t) in the post heat phase by the effective bleaching contribution $exp\left(-t \cdot k_{Bleach,effective}\right)$ and $D(t) \cdot \hat{F}_{Free}$ yields for the kinetic fluorescence term

$$F_{kinetic}(t) = \int dV \left(1 - P_{bound,eq} + \frac{\hat{F}_{Bound}}{\hat{F}_{Free}} P_{bound,eq} + \frac{\hat{F}_{Free} - \hat{F}_{Bound}}{\hat{F}_{Free}}\left(P_{bound,eq} - P_{bound,hot}\right) \cdot exp(-t/\tau_{kinetic})\right) \quad (7)$$

The right hand side of the equation has a single time-dependent term, which is the kinetic relaxation term $exp(-t/\tau_{kinetic})$. We subtracted 1 from the right hand side of Eq. 7, also see SI-Fig.2 a, and fitted an exponential function $F_{kinetic}(t) = F_{kinetic,offset} + F_{kinetic,amplitude} \cdot exp(-t/\tau_{kinetic})$ to obtain $\tau^{-1}_{kinetic}$, see Fig.3 b. The subtraction of 1 yielded for better converging fits but is in general not necessary. We did not further investigate $F_{kinetic,\ offset}$ as it carried no information of interest of the kinetic relaxation. The error of the fit is obtained by the root mean squared error times the variance of the fit.

The on-rate is fitted with a Levenberg-Marquart algorithm according to Eq. 2 for the fitted $\tau^{-1}_{kinetic}$ and respective total ligand concentrations L_{tot}. K_d and labeled binder concentration B^*_{tot} are constant for all ligand concentrations and k_{on} is the only fitting parameter. The fitting-weights ω for each data point are the inverse quadratic relative errors $\omega = \frac{1}{\Delta\tau^{-2}_{kinetic}/\Sigma\Delta\tau^{-2}_{kinetic}}$, with the fitting errors $\Delta\tau^{-1}_{kinetic}$. If a fluorescence trace did not show kinetic behavior, the fitted relative error $\frac{\Delta\tau^{-1}_{kinetic}}{\tau^{-1}_{kinetic}}$ was comparably large (>0.15). Those traces were excluded from the on-rate fit. The off-rate k_{off} was calculated by $k_{off} = K_d \cdot k_{on}$ and the error of the off-rate is obtained by Gaussian error propagation from K_d and k_{on} fits. All analysis calculations were made with LabView.

5 Rate equation simulations in 3D inside the capillary

To validate the experimentally-determined kinetic rates, we simulated the reaction kinetics with finite elements simulations (COMSOL Multiphysics). We simulated the fluorescence of the ligand-binder system with the measured kinetic rates and bleaching rates on the basis of the fluorescence model. So we could check if the analysis of the kinetic rates that resulted from the fluorescence simulations matched the empirically determined input rates of the simulations.

We modeled the species of free fluorescent label B^*, bound fluorescent label LB^*, bleached label B, bleached bound label LB and free ligand L according to the fundamental rate equation system of Eq. 4 in a glass capillary, see Fig.1 b. The geometry comprised a glass capillary (ID 300 µm, OD 400 µm), placed on a silicon block of 400 µm thickness. The cover slip is directly on top of the capillary and has a thickness of 200 µm. The space outside the capillary between silicon block and glass cover slip is filled with immersion oil. The heating IR laser heats with a gaussian beam profile (minimal width 12 µm, NA=0.12, power density 100 W/m, attenuation length 400 µm in water, no absorbance in glass/silicon, z-focus height 200 µm above the capillary center) and the LED homogeneously illuminates the capillary on a length of 400 µm.

The fluorescence parameters of the simulated 12mer in 0.1xPBS at 19°C were determined to be

$$\begin{aligned} F_{Free} &= 1 \\ F_{Bound} &= 0.9 \\ \frac{\partial F_{Free}}{\partial T} = \frac{\partial F_{Bound}}{\partial T} &= -0.026K^{-1} \\ k_{Bleach,free} &= 0.0021s^{-1} \\ k_{Bleach,bound} &= 0.0029s^{-1} \\ k_{off,offset} &= 117.890 \\ k_{off,slope} &= -36313.5K \\ k_{on} &= 3.5 \cdot 10^4 M^{-1}s^{-1} \\ B^*_{tot} &= 2nM \\ L_{tot} &= 0\mu M \wedge 2.5\mu M \\ D &= 1.5 \cdot 10^{-10}m^2s^{-1} \\ D_T &= 1.8 \cdot 10^{-12}m^2s^{-1}K^{-1} \end{aligned}$$

with the temperature off-rate of

$$k_{off}(1/T) = exp\left(k_{off,offset} + k_{off,slope} \cdot \frac{1}{T}\right) \cdot [s^{-1}]$$

Note that k_{off} used in the simulation from the k_{off}-fit is not equal to the measured k_{off} of 12mer at 19°C (k_{off}=0.017 s^{-1}) of Tab. 3. The simulation yields fluorescence traces, which are analyzed in the same way as the measured fluorescence traces. The analysis of the simulated fluorescence traces yields for values matching the experimental data (for fixed K_d=47 nM in equilibrium).

The volume force on the fluid takes light pressure and static fluid pressure into account. The simulation is conducted similar to the experiment with 50 seconds pre heat phase, 40 s heat phase and 60 s post heat phase. The simulation starts in kinetic equilibrium according to the binding curve Eq. 1. The simulation yielded kinetic rates which are in good agreement with the rates of the experiment:

$$\begin{aligned} k_{off,simulation\ result} &= 0.0016s^{-1} \\ k_{on,simulation\ result} &= 3.45 \cdot 10^4 M^{-1}s^{-1} \end{aligned}$$

6 Independence of kinetic rates on label site

In all measurements, the fluorescent label was attached to the end of the strand at which the (shorter) complementary DNA strand bound to. We measured similar kinetic rates of a fully complementary strand with distantly attached label. A complementary 12mer strand hybridizes starting at the 3' end of the Cy5-5'-16mer-3' strand, leaving a distance of 4 single strand bases between the Cy5 label (which is at the 5'end) and the hybridized strand. The measured K_d and kinetic rates of this hybridized strand with an increased distance

Kinetic rates distant fluorescent label							
		Salt 0.1xPBS					
1/T [1000/K]	Temp[°C]	K_d [nM]	Std.Dev	koff [1/s]	Std.Dev	kon [1/Ms]	Std.Dev
3,53	10						
3,49	13						
3,46	16	12,6	4,7	0,00036	0,0002	28981	9000
3,42	19						
3,39	22	176	20	0,0057	0,001	32321	5300
3,35	25	1106	270	0,039	0,01	35462	2980
3,32	28						

Table 1: K_d, off-rate and on-rate with deviations for DNA hybridization measurement of a distantly attaches fluorophore are similar to strands with closely attached fluorophores compared to Tab.3-5.

of the label to the hybridized based pairs are similar to the results of the close label. Measurements of K_d and kinetic on-rates and off-rates of complementary DNA strand with a distant fluorescent label show similar values to closely-attached fluorescent label, see Tab.1.

7 Influence of diffusion on fluorescence analysis

To test the accuracy of the analysis of the kinetic rates on the deconvolution of the diffusion contribution, we performed the analysis of the traces for 12mer at 19°C with and without diffusion correction, see SI-Fig.2. This corresponds to the scenario that the ligand is diffusing but the labeled binder would not diffuse. We found that, if the correction for backdiffusion is dropped, the resulting rates change by a factor less than two. With regard to the orders of magnitude, by which the measured kinetic rates differ within literature, the factor smaller two is comparably small. We take this finding as an indicator that the analysis method shows robust results regarding differences of diffusion properties of the binder and ligand.

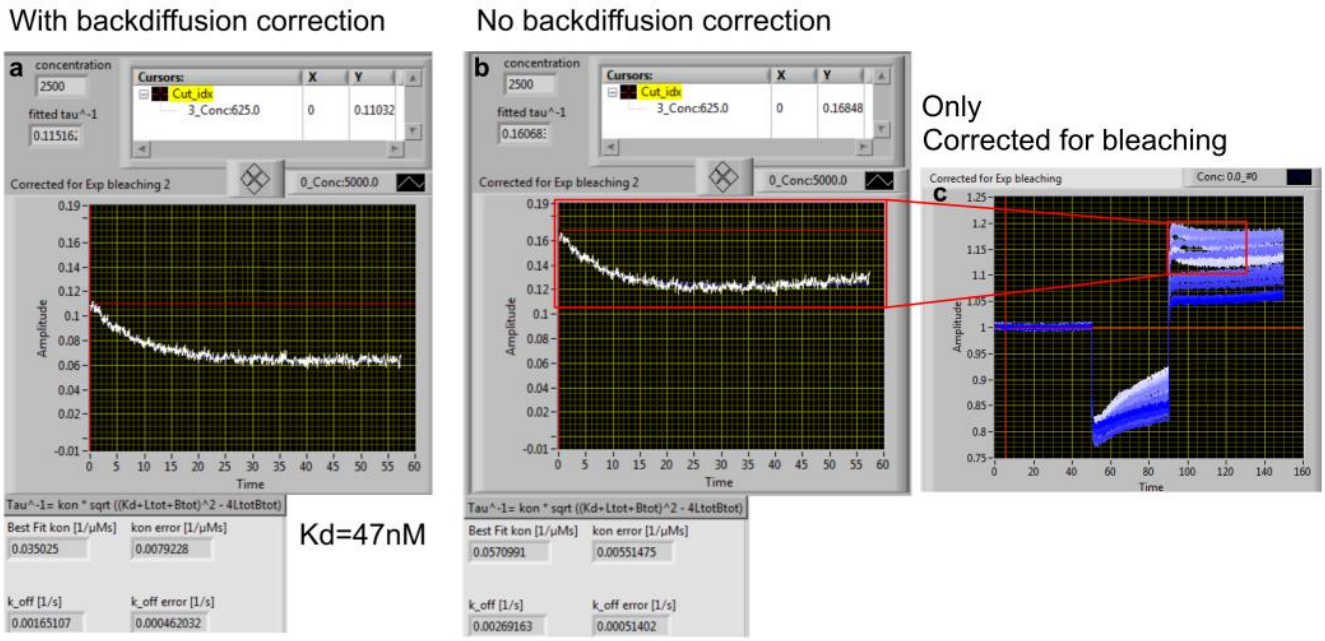

SI-Figure 2: Backdiffusion contribution to kinetic analysis a *Bleaching- and diffusion-corrected fluorescence trace of 12mer at 19°C for 2500nM ligand and 2nM binder with resulting on- and off-rate as described in SI-Sec.* ***b*** *Analysis of the same trace without backdiffusion correction, that is the division by the averaged zero-ligand trace and resulting kinetic relaxation time constant and rates.* ***c*** *Fluorescence traces with only bleaching correction but no diffusion correction.*

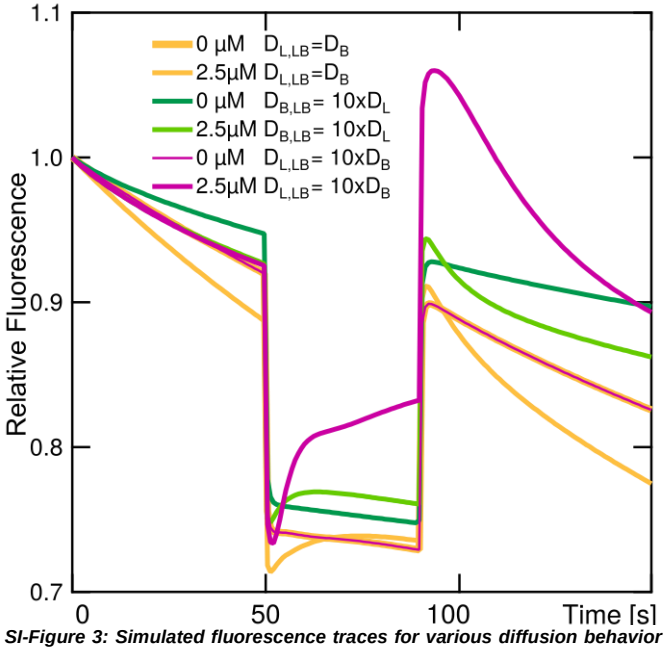

SI-Figure 3: Simulated fluorescence traces for various diffusion behavior *Simluated fluorescence traces for similar diffusion behavior (yellow), larger fluorescent binder (green) and larger fluorescent ligand (purple) for 0nM and 2500nM ligand concentration with the rates of 12mer at 19°C. The traces of the larger fluorescent binder simulations are similar to the results of equal diffusion behavior, with similar kinetic rates. For the larger ligand simulations, the labeled binder accumulates in the top center of the capillary, see SI-FigZ g and fluorescence restores quickly. The analyzed kinetic rates differ by a factor of 5 in comparison with the similar diffusion behavior simulations.*

Next, we used our 3D-Comsol simulations to test, how the fluorescence traces would look and the kinetic rates would be fitted, if one of the reactants exhibited strongly different diffusion coefficient, while the on-rate and off-rate did not change. Therefore, we simulated two cases: In the first, the ligand had tenfold increased diffusion coefficient $D_L=D_{LB}=10xD_B$, i.e. because the non-labeled ligand was much larger than the labeled binder. In the second case, the labeled binder had tenfold increased $D_B=D_{LB}=10xD_L$. In both cases, we assumed that the diffusion coefficient was the same for bound ligand LB and the respective larger free L or B, which had the higher diffusion coefficient. The diffusion behavior of the larger reactant would not change, hen bound to the much smaller reactant.

For the first case, we found that the fluorescence trace for high ligand concentration L_{tot}=2500 nM (over 1000-fold excess of binder B_{tot}=2 nM) looked significantly different for the hot phase (50-90 seconds), see purple traces SI-Fig.3. The deviation of the simulated detected fluorescence at the beginning of the hot phase, compare SI-Fig.4 a and e, can be explained by the concentrations of free L, free B* and bound LB*: During the heating time, the absolute fluorescence initially dropped due to the quick temperature change. Shortly after the temperature change, within about 10 seconds, bound complexes diffused quickly ($D_{LB}=10xD_B$) from the cold non-illuminated region ($c_{LB*}>c_{B*}$) back into the top center of the capillary (heated area, illuminated), see SI-Fig.4 b and f, and the absolute fluorescence increased quickly again. In the hot center, the bound complexes unbound, see SI-Fig.4 c and g, the fast diffusing unbound ligand molecules moved away from

the top center of the capillary, see SI-Fig.4 d and h, whereas the slowly diffusing labeled binder molecules got stuck at the top center. This left an excess of unbound labeled binder molecules in the top center of the capillary, see SI-Fig.4 c, and explained the increased

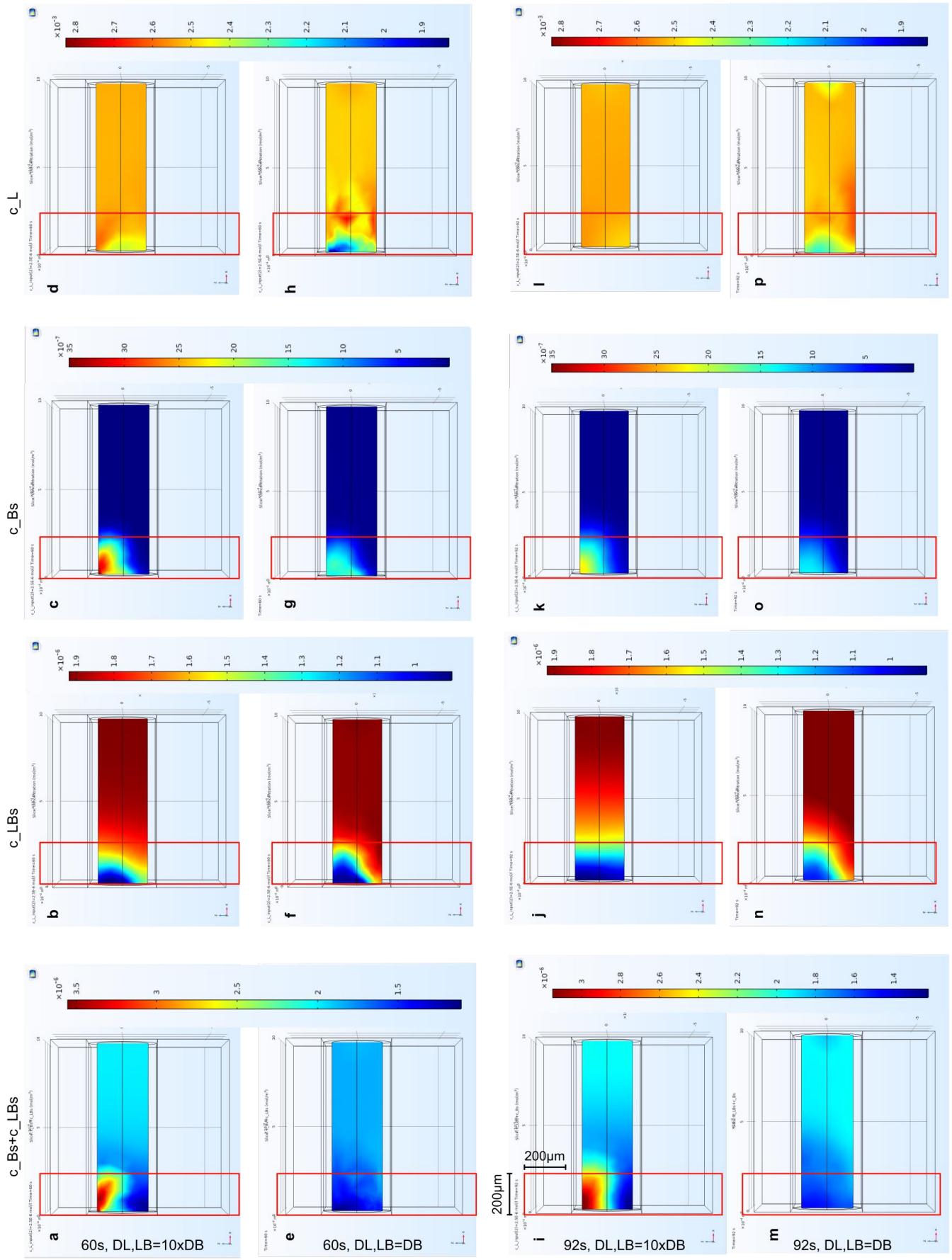

SI-Figure 4: Simulated concentrations of free L, free B* and bound LB* a-h *at 60 seconds during the hot phase and* ***i-p*** *at 92 seconds shortly after the rebinding start for Ltot=2500nM and B*tot=2nM.* ***A-d*** *and* ***i-l*** *show the concentrations for tenfold increased ligand diffusion coefficient $D_{LB^*}=D_L=10xD_B$. e-h and m-p show the concentrations for equal ligand diffusion coefficient $D_{LB^*}=D_L=D_B$. The illuminated region (200µm width) is shown by the red rectangle and shows the symmetrical half of the simulated capillary. The laser focus is on the left edge of each plot.*

absolute fluorescence (purple) in the hot phase.

When the laser was switched off, the initial absolute fluorescence level was higher due to accumulated free labeled binders in the top center capillary, see SI-Fig.3 purple line at 90 seconds and SI-Fig.4 i and m. The kinetic relaxation of rebinding free labeled binder, see SI-Fig.4 k, and free ligand see SI-Fig.4 l, yielded for slower kinetics. The analysis of the traces yielded for an on-rate $7x10^3 M^{-1}s^{-1}$, which was about one fifth of the input rate $3.5x10^4 M^{-1}s^{-1}$. The analysis of the off-rate yielded for $3.3x10^{-4} s^{-1}$ which was also about one fifth smaller than the input rate. This deviation of the analyzed kinetics from the simulations with equal diffusion behavior can be explained by the reduced homogeneously distributed free binders. In the analysis, we assume homogeneously distributed binder and ligand in the detected volume, see SI-2. But due to non-homogeneous accumulation of labeled binder in the top center, the assumption of homogeneity was not as valid as in the similar diffusion behavior simulations, see SI-Fig.4 k and l, which are less homogeneously distributed than SI-Fig.4 o and p. In the second case, the fluorescent binder had tenfold increased diffusion coefficient, e.g. a small compound that binds to a larger (labeled) protein. The simulated fluorescence trace showed less bleaching and similar behavior during the heating period and post-heating period, resulting with an on-rate of $5.6x10^4 M^{-1}s^{-1}$ and off-rate of $2.7x10^{-3}s^{-1}$. The on-rate was a factor of 1.6 higher and the off-rate a factor of 1.6 smaller than the input parameters, which is very close to the input parameters. K_d stays the same, as we only varied diffusion behavior and not binding behavior.

We interpret the variation of analyzed kinetic rates by smaller than five-fold for dissimilar diffusion behavior of the reactants as a support of our claim that our applied analysis is robust to different sizes of ligand and binder. With regard to the magnitudes of differently reported kinetic rates in literature our reported variations are comparably small. Taken together, the simulation results suggest that if the label could be attached to either the binder or the ligand, the larger molecule should be labeled to reduce systematic errors within the kinetic rate analysis.

8 Optimal conditions for KMST measurements

We could characterize four conditions for optimal applicability of KMST. First, for small equilibrium constants K_d < 1 nM, the weak fluorescence signal did not allow a reliable analysis of the data. To obtain reliable binding signals and to provide useful fitting of Eq. 1, the fluorescent label generally needed to be even smaller $B^*_{tot} < K_d$ and thus in the sub nM and pM range. Low B^*_{tot} concentrations led to low absolute fluorescence signals in the detector, which were more difficult to analyze due to a smaller signal-to-noise ratio. This limited the determination of kinetic rates. In order to increase the fluorescence level, increasing the LED excitation intensity did not solve the problem, as then bleaching was so pronounced, that triplicate measurements of a single sample capillary were not useful, due to almost completely bleached samples after the first measurement. Also, for strong bleaching, the fluorescence was strongly dominated by the bleaching component, making it difficult to differentiate the kinetic contribution from bleaching.

Second, the detection of fast kinetic relaxation of $\tau_{kinetic}^{-1} > 1s^{-1}$, e.g. for high ligand concentrations and for high on-rates, was limited by the heating, cooling and fluorescence detection time scale $\tau_{cooling}^{-1} \approx 5s^{-1}$.This was problematic for two reasons. First, the superposition of fluorescence change due to heating and kinetic relaxation became more difficult to dissect, as they were on the same timescale. Second, the assumption of an immediate temperature jump in only valid for $\tau_{kinetic}^{-1} \ll \tau_{cooling}^{-1}$ and the data analysis would need to be modified to cover time-dependent temperature equilibration with possibly the lack of an analytic description of the time constant.

Third, the KMST measurements depended on temperature-dependent binding and unbinding of biological complexes. This required a significant enthalpic contribution ΔH^0 which led to temperature-dependent K_d. Biological complexes with very weak enthalpic contribution$\Delta H \approx 0$would not change binding in the heating phase and no kinetic recombination in the post heating phase would be detected. Measurements with p38-a MapKinase with BIRB, SB203580, SB239063 (not shown) did not yield for fluorescence traces with a strong enough kinetic fingerprint, most likely due to an insufficient enthalpic contribution.

Fourth, the absolute fluorescence change upon binding required to be significant. To measure the kinetic relaxation fingerprint, a sufficient high value of $F_{kinetic,amplitude} > 0.05$ is crucial. The company Nanotemper which commercializes MST, has developed in the past dyes with ever increasing thermal binding signal, so that also in KMST, the sensitivity to measure kinetics will increase over time. The origin of the binding-dependent fluorescence intensity may play a minor role. E.g. it may stem from a change in conformation upon binding, thus the fluorophore does not necessarily need to be in close proximity to the binding site, which reduces the label influence on binding characteristics.

Additionally, KMST experiments require the system to be at kinetic equilibrium in the pre-heating phase. Therefore it has to be ensured that the sample has reached equilibrium after mixing the reactants[5] and incubating for 20 minutes. The measured relaxation time constants were in the order of 10 seconds. We draw the conclusion that the sample has equilibrated during the 20 minute incubation after capillary filling and thus the system was in equilibrium in the pre-heat phase.

9 DNA samples & preparation

Each dilution series comprises 16 vials, in a 1:1 dilution between the vials. In vial 15 and 16 only binder with no ligand is used for a the $F_{diffusion}$ measurement. The binder concentration is set below K_d to yield for binding curves to obtain reasonable K_d values. The labeled binder concentrations were set to 2nM to yield for good K_d fits as well as sufficient fluorescence counts. The range of the ligand concentration was chosen to be symmetric around K_d, to obtain a valid binding curve, reaching the unbound plateau and bound plateau for the fraction bound curve, see Fig3 b.

The DNA strands used for hybridization kinetics determination were purchased at biomers (Ulm, Germany). The fluorescent labeled binder was a 16mer sequence

Cy5-5'CCT CAT CCA TAG TTG C3'

and the complementary ligands

10mer: 5'a tgg atg agg3'

12mer: 5'cta tgg atg agg3'

12mer: 5'gca act atg gat3' only used for control with 'distantly attached label' (SI-6)
14mer: 5'aa cta tgg atg agg3'.
16mer: 5'g caa cta tgg atg agg3'.

The ligand strands bind to the binder strands at the Cy-5-End to obtain a strong binding-dependent change of the fluorescence signal. All used strands were factory HPLC purified before purchase. The stock concentration for all strands was 100µM dissolved in water (nuclease-free H_2O, Ambion). As the fluorophore is located next to the binding nucleotides, the fluorescence becomes binding-dependent, reported earlier.[6] Both strands are not self-complementary and no side reactions are expected.

The DNA strands were dissolved in 0.75x, 0.5x, 0.25x and 0.1x PBS buffer (stock: 10xPBS invitrogen ThermoFisher, diluted in nuclease-free water H_2O, Ambion). To avoid sticking of material to the capillary walls, 0.05% (wt/vol) Tween 20 (NanoTemper) was added to all buffers. The experiment ambient temperatures were chosen to be below the melting temperature T_m of the fully complementary strand to obtain a high change of fraction bound due to the temperature change. SI-Fig.5 a shows the melting curve of the 12mer in 0.1xPBS for 10µM of each the binder strand and the complementary 12mer strand. The melting curve was recorded with a thermo cycler (10°C to 90°C, Biorad, C1000 Thermal Cycler) and 1xEvaGreen intercalating dye. To correct for the temperature-related intensity change of the dye, the melting curve was divided by a curve of Eva-Green dye with 10µM binder-only (not shown). The melting temperature was 43°C, which is at least 15K above the set ambient temperature of the kinetic measurements. We conclude that the strands were bound in the pre heat and post heat phase and heating the sample with the infrared laser melted the hybridized DNA strands. When the laser was switched off, the DNA strands hybridized and kinetics were detected. Simulation of T_m for the used strands under the respective PBS buffer Na^+ conditions were rather inconclusive for low salt concentrations and short strands. The simulation of melting temperature with Oligo Calc[7] (salt adjusted and nearest neighbor mode) and NUPACK[8] are shown in Tab. 2.

T_m [°C] calculated for x PBS	0.1	0.25	0.5	0.75
12 mer NUPACK	-	-	23.5	25
12 mer Oligo Calc Nearest Neighbor	8.1	14.9	19.9	22.8
12 mer Oligo Calc salt adjusted	26.7	33.3	38.2	41.2
T_m [°C] calc. for strand lengths 0.1 x PBS	10	12	14	16
Oligo Calc nearest neighbor	-2.1	8.1	16.2	25.9
Oligo Calc salt adjusted	20.3	26.3	28.2	38.4

Table 2: Overview of calculated melting temperatures for used DNA strands

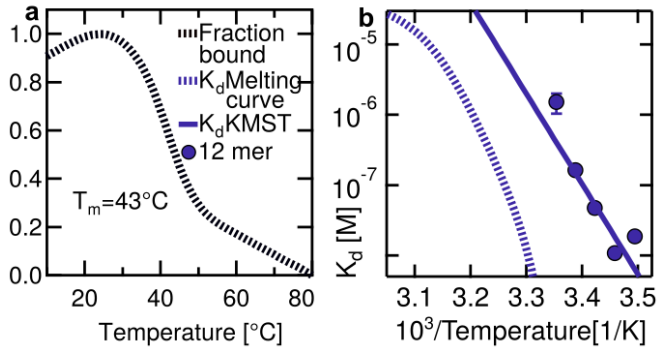

SI-Figure 5: Melting curve and Van't Hoff a *shows the melting curve (fraction bound) obtained with a Biorad Thermocycler of the 12mer in 0.1xPBS and 1x EvaGreen intercalating dye. The concentration of the labeled strand and of the complementary strand were 10µM each. The fluorescence temperature calibration was performed by division by a temperature curve of the labeled strand with Eva Green dye only.* ***b*** *shows the Van't Hoff plot of the melting curve data in comparison with the data from KMST. Both show similar slope and the melting curve data is shifted towards higher temperatures. This may stem from the fluorescence calibration of Eva Green dye. Also, at the small temperatures $T<T_m$ measured with KMST, it is difficult to determine K_d from a binding curve, as almost all strands are hybridized and the melting signal changes little at $T<T_m$.*

Results and Discussion

10 Summarized measured kinetic rates and equilibrium constant

Tables 3 – 5 show the corresponding values of the measured equilibrium constant K_d [M], k_{off} [s^{-1}] and k_{on} [$M^{-1}s^{-1}$] with respective standard deviations of Fig.4&5.

Equilibrium constant K_d									
		Salt [xPBS]							
		0.1		0.25		0.5		0.75	
1/T [1000/K]	Temp[°C]	Kd [M]	Std.Dev	Kd [M]	Std.Dev	Kd [M]	Std.Dev	Kd [M]	Std.Dev
3.53	10								
3.49	13	1.9E-8	2.6E-9						
3.46	16	1.1E-8	9.1E-10						
3.42	19	4.7E-8	7.8E-9						
3.39	22	1.6E-7	1.5E-8	1.4E-8	4.4E-9			3.9E-10	2.1E-10
3.35	25	1.5E-6	4.9E-7	5.3E-8	1.8E-8	4.7E-9	3.2E-9	6.7E-10	4.4E-10
3.32	28					1.2E-8	1.1E-8	1.0E-9	6.5E-10
		Length [#bp] in 0.1xPBS							
		10		12		14		16	
		Kd [M]	Std.Dev	Kd [M]	Std.Dev	Kd [M]	Std.Dev	Kd [M]	Std.Dev
3.53	10	4.5E-9	2.1E-9						
3.49	13	4.3E-8	1.7E-8	1.9E-8	2.6E-9				
3.46	16	1.2E-7	3.2E-8	1.1E-8	9.1E-10				
3.42	19	3.8E-7	1.9E-7	4.7E-8	7.8E-9				
3.39	22	3.9E-6	9.6E-7	1.6E-7	1.5E-8	5.1E-8	1.9E-8	1.1E-9	2.3E-10
3.35	25			1.5E-6	4.9E-7	1.1E-8	5.6E-9	7.6E-9	1.7E-9
3.32	28					2.8E-9	7.2E-10	9.4E-9	1.9E-9

Table 3: Equilibrium constant K_d [M] and standard deviation [M] for DNA hybridization measurements.

Off-rate k_{off}									
		Salt [xPBS]							
		0.1		0.25		0.5		0.75	
1/T [1000/K]	Temp[°C]	koff [1/s]	Std.Dev	koff [1/s]	Std.Dev	koff [1/s]	Std.Dev	koff [1/s]	Std.Dev
3.53	10								
3.49	13	3.7E-4	7.5E-5						
3.46	16	2.4E-4	3.0E-5						
3.42	19	1.7E-3	4.6E-4						
3.39	22	7.8E-3	1.2E-3	2.9E-3	9.7E-4			4.2E-4	2.4E-4
3.35	25	3.3E-2	1.6E-2	1.1E-2	4.1E-3	5.2E-3	4.2E-3	9.8E-4	6.5E-4
3.32	28					1.3E-2	1.5E-2	1.6E-3	1.0E-3
		Length [#bp] in 0.1xPBS							
		10		12		14		16	
		koff [1/s]	Std.Dev	koff [1/s]	Std.Dev	koff [1/s]	Std.Dev	koff [1/s]	Std.Dev
3.53	10	1.2E-4	5.6E-5						
3.49	13	7.6E-4	3.2E-4	3.7E-4	7.5E-5				
3.46	16	3.9E-3	1.1E-3	2.4E-4	3.0E-5				
3.42	19	1.7E-2	8.6E-3	1.7E-3	4.6E-4				
3.39	22	4.2E-2	1.6E-2	7.8E-3	1.2E-3	2.3E-4	6.1E-5	5.3E-5	1.1E-5
3.35	25			3.3E-2	1.6E-2	7.5E-4	3.8E-4	3.9E-4	8.6E-5
3.32	28					3.6E-3	1.5E-3	4.8E-4	1.2E-4

Table 4: Off-rate k_{off} [s^{-1}] and standard deviation [s^{-1}] for DNA hybridization measurements.

We also tried to measure the kinetic rates of the used 12mer by a quick temperature jump experiment with a thermocycler of Biorad with added EvaGreen intercalating dye. The heating characteristic was about 10 seconds for a jump from 70°C to 10°C and the technique was used earlier to obtain kinetic relaxation time constants of DNA 51mers with FRET.[9] Analysis of the EvaGreen signal did not yield for valid kinetic relaxation traces. This may stem from difficulties associated with the measurement of kinetics with Eva Green dye as well as the readout timing of the machine. Also the temperature characteristic may have been not quick enough to extract kinetics.

On-rate k_{on}									
		Salt [xPBS]							
		0.1		0.25		0.5		0.75	
1/T [1000/K]	Temp[°C]	kon [1/Ms]	Std.Dev	kon [1/Ms]	Std.Dev	kon [1/Ms]	Std.Dev	kon [1/Ms]	Std.Dev
3.53	10								
3.49	13	2.0E+4	2.8E+3						
3.46	16	2.2E+4	2.0E+3						
3.42	19	3.5E+4	7.9E+3						
3.39	22	4.8E+4	6.1E+3	2.2E+5	1.1E+4			1.1E+6	2.4E+5
3.35	25	2.2E+4	8.2E+3	2.1E+5	3.1E+4	1.1E+6	4.5E+5	1.5E+6	1.1E+5
3.32	28					1.1E+6	6.5E+5	1.6E+6	1.4E+5
		Length [#bp] in 0.1xPBS							
		10		12		14		16	
		kon [1/Ms]	Std.Dev	kon [1/Ms]	Std.Dev	kon [1/Ms]	Std.Dev	kon [1/Ms]	Std.Dev
3.53	10	2.6E+4	1.1E+3						
3.49	13	1.8E+4	1.6E+3	2.0E+4	2.8E+3				
3.46	16	3.3E+4	1.2E+3	2.2E+4	2.0E+3				
3.42	19	4.6E+4	2.7E+3	3.5E+4	7.9E+3				
3.39	22	1.1E+4	3.3E+3	4.8E+4	6.1E+3	8.4E+4	3.3E+3	4.8E+4	2.9E+3
3.35	25			2.2E+4	8.2E+3	6.6E+4	9.4E+3	5.1E+4	1.7E+3
3.32	28					7.0E+4	1.6E+4	5.2E+4	6.9E+3

Table 5: On-rate k_{on} [$M^{-1}s^{-1}$] and standard deviation [$M^{-1}s^{-1}$] for DNA hybridization measurements.

11 Van't Hoff analysis

Tab. 6 shows the fitted Van't Hoff parameters $\Delta H^0, \Delta S^0, \Delta G^0$ from the K_d plot over inverse temperature of Fig. 5 e & f. To compare the Vant'Hoff data obtained by KMST measurements with established methods, we calculated K_d over 1/T from the linear regime of the melting curve (30-55°C) by applying the fraction of bound complex P_{bound} and $K_d = \frac{L \cdot B^*}{LB^*}$ to the melting curve data, see SI-Fig.5 b. The obtained Van't Hoff plot of the melting curve data yielded for ΔH^0=-73 kcal mol^{-1} (we fitted the linear regime between 3.2-3.3x10^{-3} K^{-1}) which was in agreement with the data obtained by KMST measurements -58 kcal mol^{-1}. The shift of the Kd obtained by the melting curve and the K_d from KMST may stem from the temperature-related change of fluorescence intensity of the intercalating dye and from the fluorescence calibration of the melting curve. Also a melting curve in general is only limited suitable to extract good K_d values for temperatures well below the melting temperature $T<<T_m$ because its signal does not change significantly at $T<<T_m$, as almost all strands are hybridized. The melting curve yielded for good values in the linear regime around T_m between 30°C and 50°C. Comparing the linear regime of the melting curve with the KMST data for $T<<T_m$ yielded for good agreement.

We also tried to measure the K_d and kinetic rates with Dynamic Light Scattering (DynaPro NanoStar, Wyatt) but could not detect the probes (10µM sample concentration). Due to the small size and low concentration, the correlation function of the labeled binder could not be distinguished from the buffer-only correlation function.

In 0.1xPBS	ΔG°[a]	ΔG° stdv[b]	ΔH°	ΔH° Stdv	ΔS°	ΔS° Stdv	TΔS°
	kcal/mol	kcal/mol	kcal/mol	kcal/mol	cal/K*mol	cal/K*mol	kcal/*mol
10mer	-6.4	11.1	-86	8	-267	26	-80
12mer	-7.9	23.1	-58	16	-168	56	-50
14mer	-10.8	2.7	-85	2	-249	6	-74
16mer	-11.1	35.6	-49	25	-127	85	-38
12 mer							
0.1xPBS	-7.9	23.1	-58	16	-168	56	-50
0.25xPBS	-9.8	36.2	-79	27	-232	81	-69
0.5xPBS	-11.5	47.3	-55	37	-146	99	-44
0.75xPBS	-12.4	2.7	-27	2	-49	6	-15

Table 2: Van't Hoff parameters from Fig.5e,f. $\Delta H^0, \Delta S^0$ were fitted to $ln(K_d^0/K_d) = \frac{-\Delta H^0}{RT} + \frac{\Delta S^0}{R}$. [a] ΔG^0 was calculated and [b]the error was calculated by Gaussian error propagation. All values refer to standard temperature 298.15K.

.

12 Thermodynamic analysis

The identification of the temperature dependent kinetic rates by the Eyring-Polanyi equation allows for determination of thermodynamic quantities. Although, the connection of kinetic quantities with thermodynamic quantities depends on details of transition states[10] it is also for short oligomer hybridization of DNA, possible within limits.[11,12] Following the works of Dupuis et al.[11] he Eyring equation connects thermodynamic quantities of the binder-ligand system with the kinetic rates

$$ln(k/(\nu \cdot k^0)) = \frac{-\Delta H^{\ddagger}}{RT} + \frac{\Delta S^{\ddagger}}{R} \qquad (8)$$

with k the on-rate or off-rate, ν the attempt frequency which is implicitly temperature dependent, k^0 equals unity for the off- rate and [M^{-1}] for the on rate, $\Delta H^{\ddagger}_{on}$ the association or $\Delta H^{\ddagger}_{off}$ dissociation enthalpy and $\Delta S^{\ddagger}_{on}$ the association or $\Delta S^{\ddagger}_{off}$ dissociation entropy. The chosen identification of Eq. 8 leads to identical Eyring fits and Arrhenius fits. The thermodynamic quantities of the Eyring fits are shown in Tab. 7 for hybridization and Tab. 8 for dissociation. Note that the Arrhenius activation energy $E_{A,on}$ is identical to $\Delta H^{\ddagger}_{on}$ for the on- rate and $E_{A,off}$ is identical to $\Delta H^{\ddagger}_{off}$ for the off-rate, respectively.

The attempt frequency $\nu = 4s^{-1}$ was determined similarly to previous works of Dupuis et al.[11] whose analysis we closely follow in this section. Knowledge of the attempt frequency allows for connection of kinetic quantities with thermodynamic quantities by interpreting the pre-exponential factor of the Arrhenius equation with the entropy term of the Eyring-Polanyi equation. TST treats the hybridization of oligomer DNA strands as a one-way crossing over a transition state barrier at the attempt frequency of ν. ν is determined by diffusion limited duplex formation, which is calculated $k_{diff} = 4\pi \cdot R_{DNA} \cdot D \cdot 1000 \cdot N_A$ and has unit [$M^{-1}s^{-1}$]. The DNA radius is estimated to be 12bp times 3Å/bp and the diffusion coefficient is

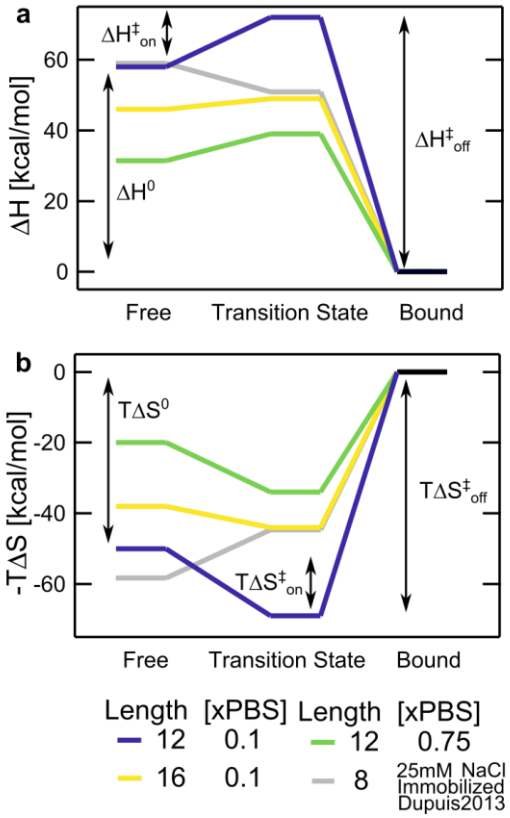

SI-Figure 6: Thermodynamic quantities of DNA hybridization for various oligomer length and salt conditions. **a** the enthalpy and **b** the entropy for free, transition and bound state. Grey data from Dupuis et al.[11]

In 0.1xPBS	$\Delta G^{\ddagger}_{off}$ [a]	$\Delta G^{\ddagger}_{off}$ stdv[b]	$\Delta H^{\ddagger}_{off}$	$\Delta H^{\ddagger}_{off}$ Stdv	$\Delta S^{\ddagger}_{off}$	$\Delta S^{\ddagger}_{off}$ Stdv	$T\Delta S^{\ddagger}_{off}$
	kcal/mol	kcal/mol	kcal/mol	kcal/mol	cal/K*mol	cal/K*mol	kcal/*mol
10mer	1.0	8.5	80	6	265	20	79
12mer	3.1	26.0	72	18	231	63	69
14mer	4.8	7.6	79	5	249	19	74
16mer	4.9	45.4	49	32	148	108	44
12 mer							
0.1xPBS	3.1	26.0	72	18	231	63	69
0.25xPBS	3.1	42.1	77	30	248	99	74
0.5xPBS	4.6	37.6	55	28	169	84	50
0.75xPBS	4.7	8.3	39	6	115	19	34

Table 7: Thermodynamic parameters for dissociation according to Eyring-plot of the off-rates of Fig.5 c & d. [a]calculated [b] estimated by Gaussian error propagation from fit. Grey values indicate an estimated error of 50% due to lack of data. TΔS is calculated for T=298K.

In 0.1xPBS	$\Delta G^{\ddagger}_{on}$ [a]	$\Delta G^{\ddagger}_{on}$ stdv[b]	$\Delta H^{\ddagger}_{on}$	$\Delta H^{\ddagger}_{on}$ Stdv	$\Delta S^{\ddagger}_{on}$	$\Delta S^{\ddagger}_{on}$ Stdv	$T\Delta S^{\ddagger}_{on}$
	kcal/mol	kcal/mol	kcal/mol	kcal/mol	cal/K*mol	cal/K*mol	kcal/*mol
10mer	-6.0	7.3	8	5	47	18	14
12mer	-6.0	7.1	14	5	67	17	20
14mer	-31.6	4.7	-8	4	79	-8	14
16mer	-5.3	5.8	3	4	28	14	8
12 mer							
0.1xPBS	-6.0	7.1	14	5	67	17	20
0.25xPBS	-6.3	24.2	-1.5	0.6	16	81	5
0.5xPBS	-7.2	3.1	-1.5	0.75	19	10	6
0.75xPBS	-7.3	5.8	7.6	4	50	14	15

Table 8: Thermodynamic parameters for hybridization according to Eyring-plot of the on-rates of Fig.5 a & b. [a]calculated [b] estimated by Gaussian error propagation from fit. Grey values indicate an estimated error of 50% due to lack of data. TΔS is calculated for T=298K.

$1x10^{-10}$ m^2s^{-1} and N_A the Avogadro Number $6.02x10^{23}$ mol^{-1}. The binder DNA concentration was 2 nM. We yield for $k_{diff}=2x10^9$ $M^{-1}s^{-1}$. To appropriately treat the diffusion constant, it is corrected by the factors T/295K and $1000/(24x10^{(247K/(T-140K))})$.[13] The factor 1000 enters because of the conversion to Molar=mol/l=1000mol/m³. Calculating $\nu_{283K} = 3s^{-1}$and $\nu_{303K} = 5.2s^{-1}$, we chose $\nu = 4s^{-1}$ for all further analysis. The uncertainties of νdo not have an influence on $\Delta H^{\ddagger}$ and E_A as they only yield for a small and logarithmic dependent shift of $\Delta S^{\ddagger}$.[11,12] As ν is a fundamental property of the transition state, it is 'almost certainly not influenced by salt type or concentration'.[12]

In order to compare the thermodynamic quantities' dependencies on salt concentrations and lengths, we plotted the enthalpy and entropy changes for the free, transition and bound state in SI-Fig.6. All changes have been referenced to the bound state. Ideally, $\Delta G^{\ddagger}{}_{on}$ and $\Delta G^{\ddagger}{}_{off}$ could be plotted to characterize DNA hybridization as a spontaneous process at the measured conditions. Unfortunately, the error of $\Delta G^{\ddagger}{}_{on}$and $\Delta G^{\ddagger}{}_{off}$are too large for a concluding remark. Our data suggests, that increasing salt concentration and increasing oligomer length favor the annealing reaction and reduce the enthalpy barrier and the entropy barrier from free to bound state.

13 Kinetic rates in crowded solutions

The kinetic rates for crowded solutions with increasing PEG 8000 concentrations are given in Tab. 9.

References

Kinetic rates PEG							
		Salt 0.1xPBS					
PEG (w/v%)	Temp[°C]	K_d [nM]	Std.Dev	koff [1/s]	Std.Dev	kon [1/Ms]	Std.Dev
0	16	11	1	0.00024	0.00005	22329	2020
	22	163	15	0.0078	0.001	47933	6114
2.5	16	7.5	2.2	0.00028	0.0001	36848	5255
	22	61	15	0.004	0.001	66762	15347
5.0	16	4.9	0.8	0.00009	0.00003	18474	4513
	22	31	5	0.0012	0.0005	39075	16174
7.5	16						
	22	59	23	0.005	0.002	83729	13299
10.0	16	36	4	0.00036	0.00004	9902	842
	22	263	56	0.007	0.002	26881	3670

Table 9: K_d, off-rate and on-rate with deviations for 12mer DNA hybridization measurement in PEG (w/v%) in 0.1xPBS

[1] C. J. Wienken, P. Baaske, U. Rothbauer, D. Braun, S. Duhr, *Nat. Commun.* **2010**, DOI 10.1038/ncomms1093.

[2] P. Baaske, C. J. Wienken, P. Reineck, S. Duhr, D. Braun, *Angew. Chemie - Int. Ed.* **2010**, *49*, 2238–2241.

[3] I. Schoen, H. Krammer, D. Braun, *Proc. Natl. Acad. Sci. U. S. A.* **2009**, *106*, 21649–21654.

[4] J. F. Eccleston, S. R. Martin, M. J. Schilstra, *Methods Cell Biol.* **2008**, *84*, 445–477.

[5] T. H. Scheuermann, S. B. Padrick, K. H. Gardner, C. A. Brautigam, *Anal. Biopchem.* **2016**, *496*, 79–93.

[6] K. Bielec, K. Sozanski, M. Seynen, Z. Dziekan, *Phys.Chem.Chem.Phys* **2019**, *21*, 10798–10807.

[7] W. A. Kibbe, *Nucleic Acids Res.* **2007**, *35*, W43–W46.

[8] J. SantaLucia, D. Hicks, *Annu. Rev. Biophys. Biomol. Struct.* **2004**, *33*, 415–440.

[9] A. Ianeselli, C. B. Mast, D. Braun, *Angew. Chemie - Int. Ed.* **2019**, *58*, 13155–13160.

[10] P. J. Doyle, A. Savara, S. S. Raiman, *React. Kinet. Mech. Catal.* **2020**, *129*, 551–581.

[11] N. F. Dupuis, E. D. Holmstrom, D. J. Nesbitt, *Biophys. J.* **2013**, *105*, 756–766.

[12] K. A. van der Meulen, S. E. Butcher, *Nucleic Acids Res.* **2012**, *40*, 2140–2151.

[13] J. Kestin, M. Sokolov, W. A. Wakeham, *J. Phys. Chem. Ref. Data* **1978**, *7*, 941–948.

Author Contributions

J.A.C.S performed the experiments, the simulations and analyzed the data. J.A.C.S, A.I and D.B. conceived and designed the experiments and simulations, and wrote the manuscript